

Effective lattice Hamiltonian for monolayer MoS₂ : Tailoring electronic structure with perpendicular electric and magnetic fields

Habib Rostami,¹ Ali G. Moghaddam,² and Reza Asgari¹

¹*School of Physics, Institute for Research in Fundamental Sciences (IPM), Tehran 19395-5531, Iran*

²*Department of physics, Institute for Advanced Studies in Basic Sciences (IASBS), Zanjan 45137-66731, Iran*

(Dated: April 11, 2022)

We propose an effective lattice Hamiltonian for monolayer MoS₂ in order to describe the low-energy band structure and investigate the effect of perpendicular electric and magnetic fields on its electronic structure. We, first, derive a tight-binding model based on the hybridization of d orbitals of Molybdenum and p orbitals of Sulfur atoms and then, introduce a modified two-band continuum model of monolayer MoS₂ by exploiting the quasi-degenerate partitioning method. Our theory reveals a difference in electron and hole masses and provides trigonal warping effects. Furthermore, we predict a valley degeneracy breaking effect in Landau levels. Besides, we also show that application of a gate field perpendicular to the monolayer, breaks the vertical mirror symmetry and induces different potentials in the three sublayers, can slightly modify the electronic structure including the band gap and effective masses.

PACS numbers: 73.22.-f, 71.18.+y, 71.70.Di, 73.63.-b

Introduction — Although studies of two dimensional (2D) electronic systems go back to some decades ago, it was only in 2004 that the first truly 2D one-atom thick material, graphene, was isolated successfully [1]. Since then the fundamental interest besides the promising applications in nanoelectronic devices, has boosted the research about atomically thin 2D materials. It has been recently demonstrated that monolayer Molybdenum Disulphide (ML-MDS), MoS₂, a prototypical transition metal dichalcogenide, shows a transition from an indirect band gap of 1.3 eV in a bulk structure to a direct band gap of 1.8 eV in the monolayer structure [2, 3]. The electronic structure of ML-MDS exhibits a valley degree of freedom indicating that the valence and conduction bands consist of two degenerate valleys (K , K') located at the corners of hexagonal Brillouin zone. The lack of inversion symmetry of ML-MDS results in a strong spin-valley coupling and the valence and conduction bands can be described by a minimal effective model Hamiltonian with a strong spin-orbit interaction which splits the valence band to spin-up and spin-down subbands [4–6]. Due to the peculiar band structure, a variety of nanoelectronic applications [7] including valleytronics, spintronics, optoelectronics and room temperature transistor [3] are suggested for ML-MDS. Induction of valley polarization using optical pumping with circularly polarized light is validated by both *ab initio* calculations and experimental observations [5, 6, 8, 9]. Also a combined valley and spin Hall physics has been predicted as a result of intimate coupling of spin and valley degrees of freedom [4].

In this letter, we propose an effective model Hamiltonian governing the low-energy band structure of monolayer dichalcogenides and show that its electronic properties can be tuned by applying a perpendicular gate voltage (PGV). Although our analysis here is focused on ML-MDS, our approach can be easily generalized to other

dichalcogenides systems MX₂. We obtain a seven band model (ignoring spin splitting) in which four of them are contributed mainly from Sulfur (S) p orbitals and three remaining mostly originated from Molybdenum (Mo) d hybrids. Our theory describes the conduction and spin-split valence bands in accordance with early theoretical studies [11], recent density functional theory calculations [12] and shows energy corrections to the band structure by trigonal warping (TW). The physics of nanoribbon, defects, impurities and so on can be studied by our lattice Hamiltonian. Intriguingly, our two-band model Hamiltonian incorporates new terms when the system is subjected to a perpendicular magnetic field. The latter gives a Zeeman-like interaction for valley which breaks the valley symmetry in contrast to [10]. Next, we introduce the effect of PGV which leads to shifts in chemical potentials of three sublayers consisting of one Mo and two S layers. We show that PGV leads to a splitting of two high energy bands originating from p orbitals of S atoms. One of our main findings is the possibility of tailoring the band gap, effective masses and the valley splitting of the valence and conduction bands by varying the induced potentials in three sublayers.

Theory and Model — ML-MDS consists of one layer of Mo atoms surrounded by two layers of S atoms in a way that each Mo atom is coordinated by six S atoms in a trigonal prismatic geometry and each S atom is coordinated by three Mo atoms. Symmetry space group of ML-MDS is D_{3h}^1 which contains the discrete symmetries C_3 (trigonal rotation), σ_v (reflection by the yz plane), σ_h (reflection by the xy plane) and any of their products [4]. In addition to the symmetry of lattice, the local atomic orbitals symmetries are essential to be considered. Trigonal prismatic symmetry dictates that d and p orbitals split into three and two groups, respectively: $\{d_{z^2}\}$, $\{d_{x^2-y^2}, d_{xy}\}$, $\{d_{xz}, d_{yz}\}$ and $\{p_x, p_y\}$, $\{p_z\}$. The

reflection symmetry along z direction allows the coupling of Mo d_{xz}, d_{yz} orbitals with only p_z orbital of S atom, whose contribution in the valence band maximum (VBM) and conduction band minimum (CBM) located at the symmetry points is negligible according to the first principal calculations [12]. Therefore CBM is mainly formed from Mo d_{z^2} orbitals and VBM is constructed by the Mo $\{d_{x^2-y^2}, d_{xy}\}$ orbitals with mixing from S $\{p_x, p_y\}$ [8, 12].

We thus can construct the tight-binding Hamiltonian for ML-MDS by using the symmetry adopted states and assuming nearest neighbor hopping terms;

$$\hat{H}_{TB} = \sum_{i\mu\nu} \{\epsilon_{\mu\nu}^a a_{i\mu}^\dagger a_{i\nu} + \epsilon_{\mu\nu}^b b_{i\mu}^\dagger b_{i\nu} + \epsilon_{\mu\nu}^{b'} b_{i\mu}^\dagger b_{i\nu}'\} + \sum_{\langle ij \rangle, \mu\nu} t_{ij, \mu\nu} a_{i\mu}^\dagger (b_{j\nu} + b_{j\nu}') + H.c., \quad (1)$$

Here $a, b(b')$ indicate the Mo and S atoms in up (down) layer, respectively. The indices μ, ν show the orbital degrees of freedom labelled as $\{1, 2, 3\} \equiv \{d_{z^2}, d_{x^2-y^2} + id_{xy}, d_{x^2-y^2} - id_{xy}\}$ and $\{1', 2'\} \equiv \{p_x + ip_y, p_x - ip_y\}$ for Mo and S atoms, subsequently. Therefore the matrices $\epsilon^a, \epsilon^b(\epsilon^{b'})$, and $t_{ij, \mu\nu} = \langle a, i, \mu | H | b, j, \nu \rangle$ are responsible for the on-site energies of Mo and S atoms, and hopping between different neighboring sites in the space of different orbitals, respectively. We do need to take into account the overlap integrals, \mathcal{S} , defined similar to the hopping terms of the Hamiltonian with elements $s_{ij, \mu\nu} = \langle a, i, \mu | b, j, \nu \rangle$.

Due to the trigonal rotational symmetry of Hamiltonian, the on-site energy matrices take the diagonal form $\epsilon_{\mu\nu}^c = \epsilon_\mu^c + U^c$ for $c := \{a, b, b'\}$, in which ϵ_μ^c shows the intrinsic value of the on-site energies for the corresponding orbital state and U^c indicates the potential shift induced by PGV. Moreover, symmetry properties of the lattice lead to only three independent on-site energies $A_1 \equiv \epsilon_1^a$, $A_2 \equiv \epsilon_2^a = \epsilon_3^a$, and $B \equiv \epsilon_{1'}^{b(\prime)} = \epsilon_{2'}^{b(\prime)}$. Accordingly the symmetries imposed by σ_v, σ_h, C_3 result in constraints on the numbers of hopping integrals (three parameters) and overlap integrals (three parameters) (see the supplementary information for details). For the sake of definiteness, we choose t_{11} , t_{22} , and t_{21} as hopping integrals and corresponding forms for overlap integral elements. A good approximation is provided by Slater-Koster method [2] in which all of the hopping and overlap integrals are written as a linear combinations of $V_{pd\sigma}$, $V_{pd\pi}$, $S_{pd\sigma}$, and $S_{pd\pi}$ where $V_{pd\sigma} = \langle \mathbf{R}', p, \sigma | H | \mathbf{R}, d, \sigma \rangle$ and $S_{pd\sigma} = \langle \mathbf{R}', p, \sigma | \mathbf{R}, d, \sigma \rangle$, for instance. To complete our effective Hamiltonian, we thus need to add spin-orbit interaction (SOI) in the model which causes spin-valley coupling in the valence band. The large SOI in ML-MDS can be approximately understood by intra atomic contribution $H_{SO} = \xi(r)\mathbf{S}\cdot\mathbf{L}$. We only consider the most important contribution of Mo atoms which gives rise to the spin-orbit coupling term $H_{SO}^{Mo} = \lambda \text{diag}\{0, s, -s\}$ in the basis of states $\{1, 2, 3\}$ where λ

is the spin-orbit coupling and $s = \pm$. To study the band structure properties provided by our tight-binding model, we find its k -space form as $\sum_{\mathbf{k}} \psi_{\mathbf{k}s}^\dagger (\mathcal{H} - E\mathcal{S}) \psi_{\mathbf{k}s}$ with $\psi_{\mathbf{k}s} = (a_{\mathbf{k}s,1}, a_{\mathbf{k}s,2}, a_{\mathbf{k}s,3}, b_{\mathbf{k}s,1'}, b_{\mathbf{k}s,2'}, b_{\mathbf{k}s,1}'', b_{\mathbf{k}s,2}'')^\top$ in which $c_{\mathbf{k}s, \mu} = \sum_i c_{is\mu} \exp(i\mathbf{k} \cdot \mathbf{R}_i)$ ($c := \{a, b, b'\}$) are the annihilation operator of electrons with momentum \mathbf{k} , spin s , and orbital degree of μ . The Hamiltonian density $\mathcal{H}_{\mathbf{k}s}$ and overlap $\mathcal{S}_{\mathbf{k}s}$ are obtained as,

$$\mathcal{H} = \begin{pmatrix} \hat{H}_a & \hat{H}_t & \hat{H}_t \\ \hat{H}_t^\dagger & \hat{H}_b & 0 \\ \hat{H}_t^\dagger & 0 & \hat{H}_{b'} \end{pmatrix}, \quad \mathcal{S} = \begin{pmatrix} 1 & \hat{S} & \hat{S} \\ \hat{S}^\dagger & 1 & 0 \\ \hat{S}^\dagger & 0 & 1 \end{pmatrix}, \quad (2)$$

with the on-site energy Hamiltonian, $\hat{H}_a = U^a \mathbb{1}_3 + \text{diag}(A_1, A_+, A_-)$, $\hat{H}_b = (B + U^b) \mathbb{1}_2$, $\hat{H}_{b'} = (B + U^{b'}) \mathbb{1}_2$, the hopping matrix,

$$\hat{H}_t = \begin{pmatrix} t_{11}f(\mathbf{k}, \omega) & -e^{-i\omega}t_{11}f(\mathbf{k}, -\omega) \\ t_{21}f(\mathbf{k}, -\omega) & t_{22}f(\mathbf{k}, 0) \\ -t_{22}f(\mathbf{k}, 0) & -e^{i\omega}t_{21}f(\mathbf{k}, \omega) \end{pmatrix}, \quad (3)$$

and overlap matrix \hat{S} is defined similar to \hat{H}_t but $t_{\mu\nu}$'s are replaced by $s_{\mu\nu}$'s. Here, $A_\pm = A_2 \pm \lambda s$ and $f(\mathbf{k}, \omega) = e^{i\mathbf{k} \cdot \boldsymbol{\delta}_1} + e^{i(\mathbf{k} \cdot \boldsymbol{\delta}_2 + \omega)} + e^{i(\mathbf{k} \cdot \boldsymbol{\delta}_3 - \omega)}$ is the structure factor with $\omega = 2\pi/3$, in-plane momentum $\mathbf{k} = (k_x, k_y)$, and $\boldsymbol{\delta}_i$ ($i = 1, 2, 3$) being the in-plane components of lattice vectors.

Generally, our tight-binding model leads to seven bands for each spin direction, however, in the absence of external bias i.e. $U^c = 0$ the symmetry between top and down S sublayers reduces the number of bands to five. Two of them correspond to the conduction and valence bands, from which we calculate the effective electron and hole masses, energy gap, and valence band edge. Moreover, since CBM mostly comes from d orbitals [12], we assume 10% mixing with p orbitals for conduction band. This provide us with five equations of seven unknown parameters based on the values obtained from *ab initio* calculations and experimental measurements. Furthermore, it is presumable to consider $s_{\mu\nu}/t_{\mu\nu} = 0.1eV^{-1}$ which reduces the number of unknowns parameters to five. We consider the energy gap $\Delta = 1.9eV$, spin-orbit coupling $\lambda = 80meV$, and effective electron and hole masses $m_e = 0.37m_0$ and $m_h = -0.44m_0$ (m_0 is the free electron mass) [14], and $E_{VBM} = -5.73eV$ [15]. Eventually, all parameters can be fixed and we then obtain the on-site energies $A_1 = -1.45eV$, $A_2 = -5.8eV$, $B = 5.53eV$ and hopping integrals $e^{i\pi/6}t_{11} = 0.82eV$, $e^{-i\pi/6}t_{21} = -1.0eV$, and $e^{-i\pi/2}t_{22} = 0.51eV$. By having these parameters, our tight-binding theory is completed.

Fig. 1 shows the band structure of ML-MDS consisting of five bands for each spin in the absence of external field. Two of them are spin polarized (dotted and dashed lines) and others are spin degenerate (solid lines). The inset reveals the spin-valley coupling of the valence band while conduction band remains spin and valley degenerate. We note that due to the limitations of our model, the high energy bands may not be comparable with those of first

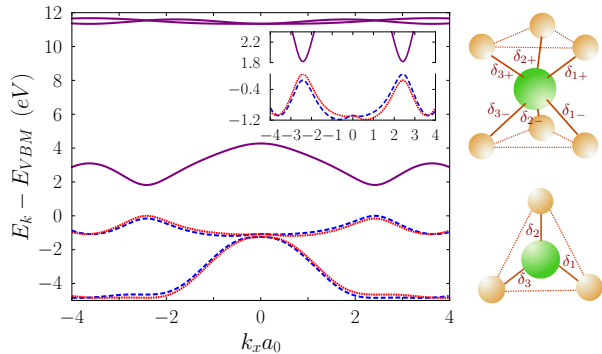


FIG. 1. (Color online) Band structure of ML-MDS consisting of five bands in which two of them are spin split in the valance band. The dotted lines refers to one spin and dashed line denotes another spin component. Solid lines refer to spin degeneracy. The inset shows a closer look to the valence and conduction bands. Here, $a_0 = a \cos(\theta)$ where a is the length of Mo-S bond and θ is the angle between the bond and $x-y$ plane. In the right panel, side and top views of the lattice structure are seen where Mo atom (larger green sphere) is surrounded by six S atoms.

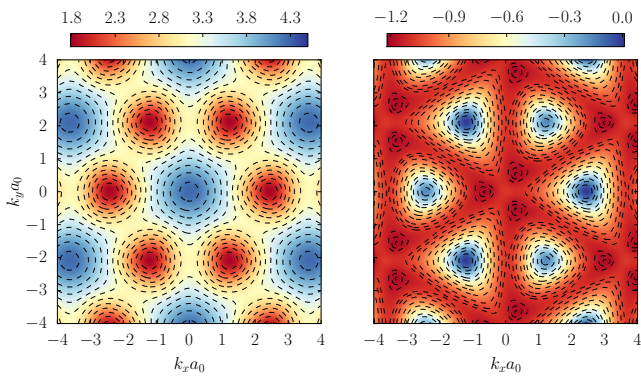


FIG. 2. (Color online) Contour plot of the conduction (left panel) and valence (right panel) bands in momentum space for spin-up component together with isoenergy lines for eye guide. While the conduction band shows almost isotropic dispersion, a strong trigonal warping is occurred in the valence band around K points and it is due to the difference of the orbital structures of the conduction and valance bands.

principal calculations in a quantitative manner. We further investigate the band structure close to the valence and conduction bands via contour plot which shows the isoenergy lines (see Fig. 2). A strong anisotropy of the constant energy lines can be seen around K points in the valence band, due to the TW, while in the conduction band all lines are almost isotropic.

The low-energy Hamiltonian — Here we present an effective low-energy two-band continuum Hamiltonian governing the conduction and valence bands around K and K' points, by exploiting the Löwdin partitioning method [17]. We first change our nonorthogonal ba-

sis ($|\psi\rangle$) to an orthogonal one ($|\psi'\rangle = \mathcal{S}^{1/2}|\psi\rangle$), leads to a standard eigenvalue problem $\tilde{H}|\psi'\rangle = E|\psi'\rangle$ with $\tilde{H} = \mathcal{S}^{-1/2}\mathcal{H}\mathcal{S}^{-1/2}$. To employ the partitioning method, we expand the new Hamiltonian up to the second order in $\mathbf{q} = \mathbf{k} - \mathbf{K}$ around $\mathbf{K} = (4\pi/3\sqrt{3}a_0, 0)$ point which can be written as the sum of q independent (\mathcal{H}_0) and q dependent (\mathcal{H}_1) parts, $\mathcal{H} = \mathcal{H}_0 + \mathcal{H}_1$. Then we rotate the orbital basis to $|\psi'_{0i}\rangle$ ($i = 1, \dots, 5$) which are the eigenstates of \tilde{H}_0 corresponding to the eigenvalues E_i 's. In the new basis, the transformed Hamiltonian is $U_0^\dagger \tilde{H} U_0$ where U_0 is the unitary diagonalizing matrix. We define two subspaces $\{|\psi'_{01}\rangle, |\psi'_{02}\rangle\}$ corresponding to the conduction and valence bands and $\{|\psi'_{03}\rangle, |\psi'_{04}\rangle, |\psi'_{05}\rangle\}$ for the three remaining bands. Then we take the block diagonal and off-diagonal parts of the Hamiltonian at these subspaces as H_{diag} and V , respectively and use the unitary transformation $H' = e^{-\mathcal{O}}U_0^\dagger \tilde{H} U_0 e^{\mathcal{O}}$ such that the lowest order in V is eliminated. This results in an effective Hamiltonian $H' = H_{\text{diag}} + [V, \mathcal{O}]/2$ which is block diagonal in the subspaces up to the second order in V .

The final result for the two-band Hamiltonian describing the conduction and valence bands reads,

$$H_{\tau s} = \frac{\Delta}{2}\sigma_z + \lambda\tau s \frac{1 - \sigma_z}{2} + t_0 a_0 \mathbf{q} \cdot \boldsymbol{\sigma}_\tau + \frac{\hbar^2 |\mathbf{q}|^2}{4m_0} (\alpha + \beta \sigma_z) + t_1 a_0^2 \mathbf{q} \cdot \boldsymbol{\sigma}_\tau^* \sigma_x \mathbf{q} \cdot \boldsymbol{\sigma}_\tau^* \quad (4)$$

for spin $s = \pm$ and valley $\tau = \pm$ in which $\boldsymbol{\sigma}_\tau = (\tau\sigma_x, \sigma_y)$, $\mathbf{q} = (q_x, q_y)$, $t_0 = 1.68\text{eV}$, $t_1 = 0.1\text{eV}$, $\alpha = 0.43$, and $\beta = 2.21$. Notice that $\alpha = m_0/m_+$ and $\beta = m_0/m_- - 4m_0v^2/(\Delta - \lambda)$ where $m_\pm = m_e m_h / (m_h \pm m_e)$ and $v = t_0 a_0 / \hbar$. The Hamiltonian differs from that of introduced by Xiao *et al.* [4] because of the second order terms in q . The diagonal q^2 terms, which contribute in the energy, in the same way as first order off-diagonal term, are responsible for the difference between electron and hole masses recently reported by using *ab initio* calculations [14]. Moreover, the last term leads to anisotropic q^3 corrections to the energy which contributes in the TW effect demonstrated in Fig. 2. Importantly, α vanishes for the case that $m_e = -m_h$, however β remains a constant.

In order to study the interplay of spin and valley physics, we introduce, by ignoring TW, the effect of time reversal symmetry breaking term by applying a perpendicular magnetic field, leading to the appearance of Landau levels (LLs) as follows,

$$E_{n, \tau s}^\pm = \pm \sqrt{\left[\frac{\Delta - \lambda\tau s}{2} + \hbar\omega_c \left(\beta n - \frac{\alpha\tau}{2} \right) \right]^2 + 2 \left(\frac{t_0 a_0}{l_B} \right)^2 n} + \frac{\lambda\tau s}{2} + \hbar\omega_c \left(\alpha n - \frac{\beta\tau}{2} \right), \quad (5)$$

where $\omega_c = eB/2m_0$ and $l_B = \sqrt{\hbar/(eB)}$ are cyclotron frequency and magnetic length, respectively. In contrast

to the study of [10], we see a new valley degeneracy breaking term which is the reminiscence of the Zeeman like coupling for valleys. As a result, the conduction band LLs are valley polarized and the valence band LLs are both valley and spin polarized although we have not yet considered the usual Zeeman interaction for spins. In addition, the $n = 0$ LL, $E_{0,\tau s}^+ = [\Delta - \hbar\omega_c\tau(\beta + \alpha)]/2$ and $E_{0,\tau s}^- = \lambda\tau s - [\Delta + \hbar\omega_c\tau(\beta - \alpha)]/2$, depend on the magnetic field strength in an opposite way for two valleys. More intriguingly, the splitting of LL in the conduction and valence bands $\delta E^+ \approx 5.4\hbar\omega_c$ and $\delta E^- \approx 4.6\hbar\omega_c$, differ with each other due to difference of m_e and $-m_h$. Furthermore, we can define three extra splitting terms for each LL in the conduction and valence bands: valley splitting $\delta E_v^+ = E_{-,s}^+ - E_{+,s}^+ \approx 2.6\hbar\omega_c$, spin splitting $\delta E_s^+ = E_{\tau,-}^+ - E_{\tau,+}^+ \approx 2\hbar\omega_c$, and spin-valley splitting $\delta E_{s-v}^+ = E_{-,-}^+ - E_{+,-}^+ \approx 3.8\hbar\omega_c$. The first and second splitting, present in the conduction band, originate from the Zeeman interactions for valleys and spins, respectively, but the latest comes from both Zeeman terms assisting each other in the valence band.

Incidentally, it is important to investigate the tunability of electronic structure via external PVG. The vertical bias breaks the mirror symmetry σ_h and modify the on-site energies of atoms in three sublayers of ML-MDS. Accordingly, these changes affect the whole electronic structure especially the low-energy characteristics such as Δ , m_e , m_h and effective hopping t_0 . Interestingly enough, tuned α and β due to PVG, can be used to emphasize the valley degeneracy breaking when the system is subjected to a perpendicular magnetic field. We assume a single-gated device in which the induced potentials take the values $U^b = 0$ and $U^{b'} = 2U^a$. The variation of mentioned parameters with the induced potential $U^{b'}$ are shown in Fig. 3, where we only illustrate the low-energy band structure for different $U^{b'}$ values. Using simple electrostatic arguments, the induced potentials for an applied vertical bias V_g can be estimated as $U^{b'} = \gamma eV_g$ with $\gamma \approx (d/L)\epsilon'/\epsilon$ where ϵ , d and ϵ' , L indicate the dielectric constants and thicknesses of ML-MDS and the substrate, respectively. For typical values $\epsilon \approx 6$ [18], $\epsilon' \approx 3.9$, $d \approx 0.32nm$, and $L \approx 300nm$ with SiO_2 as a dielectric substrate, we obtain $\gamma \approx 0.0007$. By replacing the substrate with high- ϵ gate dielectrics like HfO_2 with $\epsilon' \approx 25$ [19], the coefficient $\gamma \approx 0.004$ increases and leads to $U^{b'} \approx 0.4eV$ for $V_g = 100V$ which is already used in on-going experiments. Consequently, the PGV effects are enhanced by using a proper substrate with large dielectric constant.

It should be noted that the tight-binding model presented here with the parameters fitted empirically takes advantage of certain simplifications. First, we have neglected s , p_z orbitals of S atom and s , d_{yz} , d_{xz} orbitals of Mo atom mainly because of the symmetry arguments and the range of energies which we are interested in. Con-

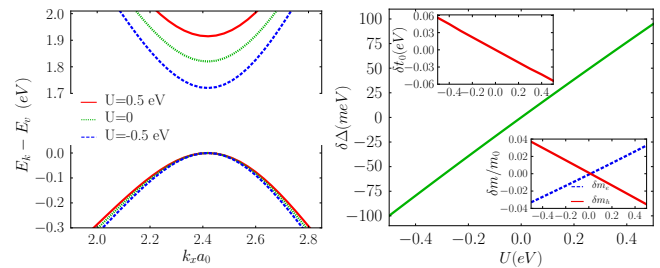


FIG. 3. (Color online) (Left panel) Spin-up conduction and valence energy bands, referred to energy $E_v = E_{VBM} + U/2$, for different vertical bias values. The conduction band is mostly affected by induced potential $U = U^{b'}$. (Right panel) Variation of the gap value versus induced potential which is almost linear in the chosen range of U . Insets show the change in the effective hopping integral and the effective masses with U . Using the form of U -dependence of the parameters, we can also estimate the linear change of $\delta\alpha \approx -0.15U/eV$ and $\delta\beta \approx -1.95U/eV$.

sequently, our model will be appropriate mostly for the low-energy calculations in the vicinity of the conduction and valence bands. Another important simplification is the ignoring of 12% ionic contribution in Mo-S bonds [16].

Conclusions — We formulated a tight-binding Hamiltonian in order to describe the low-energy band structure of monolayer MoS_2 which can be useful to study energy dispersion and transport phenomena in nanostructures MoS_2 . Our model not only successfully reproduces the low-energy dispersion of monolayer MoS_2 , but also predicts the difference in the effective hole and electron masses and the trigonal warping effect. In addition, the modified two-band model leads to a valley degeneracy breaking effect in the Landau levels. Finally, we show by applying a perpendicular electric field to the monolayer, which induces some excess charges in one Mo and two S layers that, the electronic structure especially the band gap and effective electron and hole masses can be finely tuned.

-
- [1] K. S. Novoselov, et al., *Science* **306**, 666 (2004).
 - [2] K. F. Mak, et al., *Phys. Rev. Lett.* **105**, 136805 (2010); A. Splendiani, et al., *Nano Lett.* **10**, 1271 (2010); T. Korn, et al., *Appl. Phys. Lett.* **99**, 102109 (2011).
 - [3] B. Radisavljevic, et al., *Nature Nanotech.* **6**, 147 (2011).
 - [4] D. Xiao, et al., *Phys. Rev. Lett.* **108**, 196802 (2012).
 - [5] H. Zeng, et al., *Nature Nanotech.* **7**, 490 (2012).
 - [6] T. Cao, et al., *Nature Commun.* **3**, 887 (2012).
 - [7] Qing Hua Wang, et al., *Nature nanotech.* **7**, 699 (2012).
 - [8] G. Sallen et al., *Phys. Rev. B* **86**, 081301(R) (2012).
 - [9] K. Behnia, *Nature Nanotech.* **7**, 488 (2012); S. Wu, et al., *Nature Phys.* DOI:10.1038 (2013).
 - [10] X. Li, F. Zhang, and Q. Niu, arXiv:1207.1205 (2012).
 - [11] R. A. Bromley, R. B. Murray, and A. D. Yoffe, *J. Phys. C* **5**, 759 (1972); L. F. Mattheiss, *Phys. Rev. B* **8**, 3719

- (1973); D. W. Bullett, *J. Phys. C* **11**, 4501 (1978).
- [12] E. S. Kadantsev, P. Hawrylak, *Solid State Commun.* **152**, 909 (2012); H. Shi, H. Pan, Y.-W. Zhang, B. I. Yakobson, arXiv:1211.5653; J. K. Ellis, M. J. Lucero, and G. E. Scuseria, *Appl. Phys. Lett.* **99**, 261908 (2011); C. Ataca, H. Şahin and, S. Ciraci, *J. Phys. Chem. C* **116**, 8983 (2012); S. Lebègue and O. Eriksson, *Phys. Rev. B* **79**, 115409 (2009); Z. Y. Zhu, Y. C. Cheng, and U. Schwingenschlögl, *ibid* **84**, 153402 (2011); D. Le, D. Sun, W. Lu, L. Bartels, and T. S. Rahman, *ibid* **85**, 075429 (2012); T. Cheiwchanchamnangij and W. R. L. Lambrecht, *ibid* **85**, 205302 (2012); A. Ramasubramaniam, *ibid* **86**, 115409 (2012); J. Kang, et al., *Appl. Phys. Lett.* **102**, 012111 (2013).
- [13] J. C. Slater and G. F. Koster, *Phys. Rev.* **94**, 1498 (1954).
- [14] H. Peelaers and C. G. Van de Walle, *Phys. Rev. B* **86**, 241401(R) (2012).
- [15] Yunguo Li, et al., arXiv:1211.4052 (2012).
- [16] S. P. Hind and P. M. Lee, *J. Phys. C* **13** 349 (1980).
- [17] R. Winkler, *Spin Orbit Coupling Effects in Two-Dimensional Electron and Hole Systems* (Springer, Berlin, 2003).
- [18] X. Zhang, D. O. Hayward, and D. M. P. Mingos, *Catalyst Lett.* **84**, 225 (2002).
- [19] G. D. Wilka, R. M. Wallaceb, *Appl. Phys. Rev.* **89**, 5243 (2001).

SUPPLEMENTARY MATERIAL

Seven-bands Hamiltonian

We start constructing an effective tight-binding model for a monolayer MoS₂ system, assuming the following basis orbitals,

$$\begin{aligned} |1\rangle &= d_{z^2}, \\ |2\rangle &= \frac{1}{\sqrt{2}}(|d_{x^2-y^2}\rangle + i|d_{xy}\rangle), \quad |1'\rangle = \frac{1}{\sqrt{2}}(|p_x\rangle + i|p_y\rangle) \\ |3\rangle &= \frac{1}{\sqrt{2}}(|d_{x^2-y^2}\rangle - i|d_{xy}\rangle), \quad |2'\rangle = \frac{1}{\sqrt{2}}(|p_x\rangle - i|p_y\rangle). \end{aligned} \quad (6)$$

The Wannier functions for different lattice sites in a crystal are localized and here, they can be written as $|c, i, \mu\rangle = c_{i\mu}^\dagger |0\rangle$ where i denotes the site and μ indicates atomic orbital. $c = a$ or (b, b') shows the annihilation operator of three different sublattices of monolayer MoS₂, consisting of one Mo and two S atoms. Up to the nearest-neighbor hopping integral, the tight binding Hamiltonian can be written as Eq. (1) in the letter,

$$\begin{aligned} \epsilon_{\mu\nu}^c &= \langle c, i, \mu | H | c, i, \nu \rangle, \\ t_{ij, \mu\nu} &= \langle a, i, \mu | H | b(b'), j, \nu \rangle, \\ s_{ij, \mu\nu} &= \langle a, i, \mu | b(b'), j, \nu \rangle. \end{aligned} \quad (7)$$

The lattice has two important symmetries $C_3 = e^{-i\omega L_z/\hbar}$ and $\sigma_v : \{(x, y, z) \rightarrow (-x, y, z)\}$ where the first one is the trigonal rotational symmetry operator with $\omega = 2\pi/3$ and L_z is the z -component of orbital angular

momentum and the second symmetry indicates the reflection symmetry with respect to $y-z$ plane. The act of these symmetry operators on the basis functions can be summarized in the following equations:

$$\begin{aligned} C_3\{|2\rangle, |2'\rangle\} &= e^{i\omega}\{|2\rangle, |2'\rangle\}, \quad C_3\{|3\rangle, |1'\rangle\} = e^{-i\omega}\{|3\rangle, |1'\rangle\} \\ \sigma_v\{|1\rangle, |2\rangle, |3\rangle\} &= \{|1\rangle, |3\rangle, |2\rangle\}, \quad \sigma_v\{|1'\rangle, |2'\rangle\} = -\{|2'\rangle, |1'\rangle\} \end{aligned} \quad (8)$$

and $C_3|1\rangle = |1\rangle$. It should be noticed that, here, we have dropped the spin indices. The symmetry relations in Eq. (8), impose some constraints on on-site energies and hopping integrals, and thus we have

$$\begin{aligned} \epsilon^a &= \begin{pmatrix} A_1 & 0 & 0 \\ 0 & A_2 & 0 \\ 0 & 0 & A_2 \end{pmatrix}, \quad \epsilon^b = \epsilon^{b'} = \begin{pmatrix} B & 0 \\ 0 & B \end{pmatrix}, \\ t_{\delta_{1\pm}} &= \begin{pmatrix} t_{11} & -e^{-i\omega}t_{11} \\ t_{21} & t_{22} \\ -t_{22} & -e^{i\omega}t_{21} \end{pmatrix}, \quad t_{\delta_{2\pm}} = \begin{pmatrix} e^{i\omega}t_{11} & -e^{i\omega}t_{11} \\ e^{-i\omega}t_{21} & t_{22} \\ -t_{22} & -e^{-i\omega}t_{21} \end{pmatrix}, \\ t_{\delta_{3\pm}} &= \begin{pmatrix} e^{-i\omega}t_{11} & -t_{11} \\ e^{i\omega}t_{21} & t_{22} \\ -t_{22} & -t_{21} \end{pmatrix}. \end{aligned} \quad (11)$$

Note that the same relations can be found for $s_{\delta_{i\pm}}$ by substituting $t_{\mu\nu}$'s with $s_{\mu\nu}$'s. In the presence of spin-orbit interaction of Mo atoms, it is easy to generalize ϵ^a by replacing $(\epsilon^a)_{22} \rightarrow A_2 + \lambda s$ and $(\epsilon^a)_{33} \rightarrow A_2 - \lambda s$. The subindexes of the hopping matrices indicate the nearest-neighbor vectors,

$$\begin{aligned} \delta_{1\pm} &= a\left(\frac{\sqrt{3}}{2}\cos\theta, -\frac{1}{2}\cos\theta, \pm\sin\theta\right), \\ \delta_{2\pm} &= a(0, \cos\theta, \pm\sin\theta), \\ \delta_{3\pm} &= a\left(\frac{-\sqrt{3}}{2}\cos\theta, -\frac{1}{2}\cos\theta, \pm\sin\theta\right), \end{aligned} \quad (12)$$

where $a = 2.43\text{\AA}$ and $\theta = 40.7$ degree [1] are the Mo-S bond length and the angle between the bond and Mo's plane, respectively. To find above equations, we also used the operation of C_3 and σ_v on $\delta_{i\pm}$ as $C_3\delta_{1\pm} = \delta_{2\pm}$, $C_3\delta_{2\pm} = \delta_{3\pm}$, $\sigma_v\delta_{1\pm} = \delta_{3\pm}$ and $\sigma_v\delta_{2\pm} = \delta_{2\pm}$.

Following a method proposed by Slater and Koster [2] (SK), all hopping and overlap integrals can be written as linear combinations of $V_{pd\sigma}$ and $V_{pd\pi}$ and $S_{pd\sigma}$ and $S_{pd\pi}$. In this method, we define some standard hopping and overlap parameters as $V_{l'l'|m} = \langle \vec{R}', l', m | H | \vec{R}, l, m \rangle$ and $S_{l'l'|m} = \langle \vec{R}', l', m | \vec{R}, l, m \rangle$ where $m = 0, 1$ stands for σ, π bond and other hopping and overlap integrals can be found from SK table [2]. In this way we find

$$\begin{aligned} t_{11} &= -\frac{1}{\sqrt{2}}(n_x + in_y)[\sqrt{3}n_z^2V_{pd\pi} + \frac{1}{2}(1 - 3n_z^2)V_{pd\sigma}], \\ t_{21} &= \frac{1}{2}(n_x - in_y)\left[\frac{\sqrt{3}}{2}V_{pd\sigma}(1 - n_z^2) + V_{pd\pi}(1 + n_z^2)\right], \\ t_{22} &= \frac{1}{2}(n_x - in_y)^3\left(\frac{\sqrt{3}}{2}V_{pd\sigma} - V_{pd\pi}\right), \end{aligned} \quad (13)$$

where $\mathbf{n} = (n_x, n_y, x_z)$ is a unit vector along pointing between the nearest-neighbor lattice points. Once again, we can obtain similar relations for the overlaps by substituting the hopping matrix elements with those of overlap matrix. These relations help us to reduce the number of independent hopping parameters from three to two. In the absence of external bias, due to the symmetry between two Sulfur sublattices, we can simply reduce the

7×7 Hamiltonian to a 5×5 as below

$$\mathcal{H} = \begin{pmatrix} \hat{H}_a & 2\hat{H}_t \\ 2\hat{H}_t^\dagger & 2\hat{H}_b \end{pmatrix}, \quad \mathcal{S} = \begin{pmatrix} 1 & 2\hat{S} \\ 2\hat{S}^\dagger & 2 \end{pmatrix}. \quad (14)$$

To find unknown parameters, we should first obtain the energy bands around the K -point. After solving a generalized eigenvalue problem as $\mathcal{H}|\psi\rangle = E\mathcal{S}|\psi\rangle$ at K -point, we can find the energies as

$$\begin{aligned} E_1 &= A_+, \\ E_2 &= \frac{(A_1 + B)/2 - 18\Re e(t_{11}s_{11}^*) - \sqrt{[(A_1 + B)/2 - 18\Re e(t_{11}s_{11}^*)]^2 + (1 - 18|s_{11}|^2)(18|t_{11}|^2 - A_1B)}}{1 - 18|s_{11}|^2}, \\ E_3 &= \frac{(A_- + B)/2 - 18\Re e(t_{21}s_{21}^*) - \sqrt{[(A_- + B)/2 - 18\Re e(t_{21}s_{21}^*)]^2 + (1 - 18|s_{21}|^2)(18|t_{21}|^2 - A_-B)}}{1 - 18|s_{21}|^2}, \\ E_4 &= \frac{(A_1 + B)/2 - 18\Re e(t_{11}s_{11}^*) + \sqrt{[(A_1 + B)/2 - 18\Re e(t_{11}s_{11}^*)]^2 + (1 - 18|s_{11}|^2)(18|t_{11}|^2 - A_1B)}}{1 - 18|s_{11}|^2}, \\ E_5 &= \frac{(A_- + B)/2 - 18\Re e(t_{21}s_{21}^*) + \sqrt{[(A_- + B)/2 - 18\Re e(t_{21}s_{21}^*)]^2 + (1 - 18|s_{21}|^2)(18|t_{21}|^2 - A_-B)}}{1 - 18|s_{21}|^2}. \end{aligned} \quad (15)$$

These eigenvalues include bonding (with the low-energy) and anti-bonding (with the high-energy) of $p - d$ bands. Since the conduction and valence bands are mostly formed from d_{z^2} and $d_{x^2-y^2} + id_{xy}$ orbital of Mo, therefore, E_1 and E_2 are the valence band maximum and the conduction band minimum located at K -point, respectively.

Two-bands Hamiltonian

Here, we find the low-energy two-band effective Hamiltonian with Löwdin partitioning method [3]. As de-

scribed in the text, we change nonorthogonal basis to an orthogonal one and then rotate them by using a unitary transformation, U_0 , which diagonalize \tilde{H}_0 so that to reach the new Hamiltonian,

$$H = U_0^\dagger \mathcal{S}^{-1/2} \mathcal{H} \mathcal{S}^{-1/2} U_0, \quad (16)$$

where $\mathcal{H} = \mathcal{H}_0 + \mathcal{H}_1$ and up to the second order in $q = q_x + iq_y$, \mathcal{H}_1 is given by

$$\mathcal{H}_1(\mathbf{q}) = \begin{pmatrix} 0 & 0 & 0 & -\frac{3}{2}e^{i\omega}t_{11}|q|^2a_0^2 & -3e^{i\omega}t_{11}qa_0 \\ 0 & 0 & 0 & 3e^{i\omega}t_{21}qa_0 & -3t_{22}q^*a_0 \\ 0 & 0 & 0 & 3t_{22}q^*a_0 & -\frac{3}{2}e^{-i\omega}t_{21}|q|^2a_0^2 \\ -\frac{3}{2}e^{-i\omega}t_{11}^*|q|^2a_0^2 & 3e^{-i\omega}t_{21}^*q^*a_0 & 3t_{22}^*qa_0 & 0 & 0 \\ -3e^{-i\omega}t_{11}^*q^*a_0 & -3t_{22}^*qa_0 & -\frac{3}{2}e^{i\omega}t_{21}^*|q|^2a_0^2 & 0 & 0 \end{pmatrix}, \quad (17)$$

where $a_0 = a \cos(\theta)$. In order to find the unitary transformation matrix, eigenvectors of $\tilde{H}_0 = S_0^{-1/2} \mathcal{H}_0 S_0^{-1/2}$ might be obtained first. Fortunately, $S_0^{-1/2}$ can be analytically calculated at K -point, however, for nonzero values of q , an iterative method [4] should be used. Therefore, in the vicinity of the K -point, we can treat \mathcal{H}_1 as a perturbation by assuming small enough q values and the transformed Hamiltonian, H , can be expressed as the

sum of two parts where V is a perturbation term,

$$\begin{aligned} H_{\text{diag}} &= \begin{pmatrix} h_{11}[2 \times 2] & 0 \\ 0 & h_{22}[3 \times 3] \end{pmatrix}, \\ V &= \begin{pmatrix} 0 & h_{12}[2 \times 3] \\ h_{12}^\dagger[3 \times 2] & 0 \end{pmatrix}. \end{aligned} \quad (18)$$

Now, we can employ the quasi-degenerate perturbation theory that is based on the idea of constructing a uni-

tary operator $e^{-\mathcal{O}}$ in such a way to drop the first-order V in the transformed Hamiltonian, $H' = e^{-\mathcal{O}}He^{\mathcal{O}} = H_{\text{diag}} + V + [H_{\text{diag}}, \mathcal{O}] + [V, \mathcal{O}] + \frac{1}{2}[[H_{\text{diag}}, \mathcal{O}], \mathcal{O}] + \dots$. This imposes the constraint $V + [H_{\text{diag}}, \mathcal{O}] = 0$ which leads to the following form for the generator of the transformation,

$$\mathcal{O} = \begin{pmatrix} 0 & \eta[2 \times 3] \\ -\eta^\dagger[3 \times 2] & 0 \end{pmatrix}, \quad (19)$$

with the property in which $\eta h_{22} - h_{11}\eta = h_{12}$. Then $H' = H_{\text{diag}} + \frac{1}{2}[V, \mathcal{O}] + \dots$ is an effective Hamiltonian with two decoupled subspaces. Following straightforward calculations, the effective Hamiltonian of the low-energy bands can be obtained as follows

$$h_{11} - \frac{1}{2}\{\eta h_{12}^\dagger + h_{12}\eta^\dagger\}. \quad (20)$$

Insertion of matrix form of operators h_{11} , h_{12} , and η results in the two-band form proposed in Eq. (4) in the text as

$$H_{\tau s} = \frac{\Delta}{2}\sigma_z + \lambda\tau s \frac{1 - \sigma_z}{2} + t_0 a_0 \mathbf{q} \cdot \boldsymbol{\sigma}_\tau + \frac{\hbar^2 |\mathbf{q}|^2}{4m_0} (\alpha + \beta\sigma_z) + t_1 a_0^2 \mathbf{q} \cdot \boldsymbol{\sigma}_\tau^* \sigma_x \mathbf{q} \cdot \boldsymbol{\sigma}_\tau^* \quad (21)$$

for spin $s = \pm$ and valley $\tau = \pm$.

-
- [1] Q. Yue, et al., Phys. Lett. A **376**, 1166 (2012).
 - [2] J. C. Slater and G. F. Koster, Phys. Rev. **94**, 1498 (1954).
 - [3] R. Winkler, *Spin Orbit Coupling Effects in Two-Dimensional Electron and Hole Systems* (Springer, Berlin, 2003).
 - [4] Eugene D. Denman, Alex N. Beavers, Applied Mathematics and Computation **2**, 63 (1976) .